The Astrophysical Journal, 889:135 (7pp), 2020 February 1 https://doi.org/10.3847/1538-4357/ab55de

Radius-to-frequency Mapping and FRB Frequency Drifts

Maxim Lyutikov
Department of Physics and Astronomy, Purdue University, 525 Northwestern Avenue, West Lafayette, IN, 47907, USA
Received 2019 September 23; revised 2019 November 6; accepted 2019 November 7; published 2020 January 31

Abstract

We build a model of radius-to-frequency mapping in magnetospheres of neutron stars and apply it to frequency drifts observed in fast radio bursts (FRBs). We assume that an emission patch propagates along the dipolar magnetic field lines, producing coherent emission with frequency, direction, and polarization defined by the local magnetic field. The observed temporal evolution of the frequency depends on the relativistic effects of time contraction and the curvature of the magnetic field lines. The model generically produces linear scaling of the drift rate, $\dot{\omega} \propto -\omega$, matching both numerically and parametrically the rates observed in FBRs; a more complicated behavior of $\dot{\omega}$ is also possible. Fast rotating magnetospheres produce higher drifts rates for similar viewing parameters than the slowly rotating ones. In the case of repeaters, the same source may show variable drift patterns depending on the observing phase. We expect rotational of polarization position angle through a burst, though by smaller amount than in radio pulsars. All of these findings compare favorably with properties of FBRs, strengthening their possible loci in the magnetospheres of neutron stars.

Unified Astronomy Thesaurus concepts: Radio transient sources (2008); Neutron stars (1108); Pulsars (1306); Magnetars (992)

1. Introduction

Fast radio bursts (FRBs; Lorimer et al. 2007; Cordes & Chatterjee 2019; Petroff et al. 2019) are a recently identified enigmatic astrophysical phenomena. A particular subclass of FRBs—the repeating FRBs—show similar downward drifting features in their dynamic spectra: FRB 121102 (Hessels et al. 2019), FRB 180814 (The CHIME/FRB Collaboration et al. 2019a), and lately numerous FRBs detected by CHIME (Josephy et al. 2019; The CHIME/FRB Collaboration et al. 2019b). The properties of the drifting features are highly important for the identification of the loci of FRBs, as discussed by Lyutikov (2019b).

First, the generation of narrow spectral features is natural in the "plasma laser" concept of coherent emission generation, either due to the discreteness of plasma normal modes related to the spatially local plasma parameters (e.g., plasma and cyclotron frequencies) or changing resonant conditions. Frequency drift then reflects the propagation of the emitting particles in changing magnetospheric conditions, similar to what is called "radius-to-frequency mapping" in pulsar research (e.g., Manchester & Taylor 1977; Phillips 1992).

Second, drift rates and their frequency scaling can be used to infer the physical size of the emitting region (Lyutikov 2019b). Josephy et al. (2019; see also Hessels et al. 2019) cite a drift rate for FRB 121102 of

$$\partial_t \ln \omega \approx -150 \ \mathrm{s}^{-1} \tag{1}$$

extending for an order of magnitude in frequency range. This implies that (i) emission properties are self-similar (e.g., power-law scaled) and (ii) of a typical size:

$$\Delta r \sim \frac{c}{\partial_t \ln \omega} = 2 \times 10^8 \ \mathrm{cm}. \tag{2}$$

Both these estimates are consistent with emission been produced in magnetospheres of neutron star.

In this paper, we build a model of radius-to-frequency mapping for (coherent) emission generated by relativistically moving sources in magnetospheres of neutron star. The concept of "radius-to-frequency mapping" originates in pulsar research (e.g., Manchester & Taylor 1977; Phillips 1992). The underlying assumption is that at a given place in the magnetospheres of pulsars, the plasma produces emission specified by the local, radius-dependent properties. This general concept does not specify a particular emission mechanism, it just assumes that the properties are radius dependent.

As a working model, we accept the "magnetar radio emission paradigm," in which the coherent emission is magnetically powered, similar to solar flares, as opposed to rotationally powered in the case of pulsars (Lyutikov 2002; Popov & Postnov 2013). Recently, Maan et al. (2019) discussed how many properties of magnetar radio emission resemble those of FRBs (except the frequency drifts; see Section 2.3.1)

Rotationally powered FRB emission mechanisms (e.g., as analogs of Crab giant pulses; Lyutikov et al. 2016) are excluded by the localization of the Repeating FRB at $\sim$1 Gpc (Spitler et al. 2016), as discussed by Lyutikov (2017). Magnetically powered emission has some observational constraints, but remains theoretically viable (Lyutikov 2019a, 2019b).

Within the "magnetar radio emission paradigm," the coherent emission is generated on closed field lines, presumably due to reconnection events in the magnetosphere. The observed properties then depend on (i) the particular scaling of the emitted frequency ω on the emission radius $r_{\rm em}$—$\omega(r_{\rm em})$—we leave this dependence unspecified; (ii) the motion of the emitter—we assume motion along the magnetic field line; (iii) the emission beam—we assume that emission is along the local magnetic field lines; and (iv) the line of sight (LOS) through the spinning magnetosphere.

In this paper, we consider all the above effects. First, in Section 2.2, we consider stationary magnetospheres; in Section 2.3, we consider spinning ones.

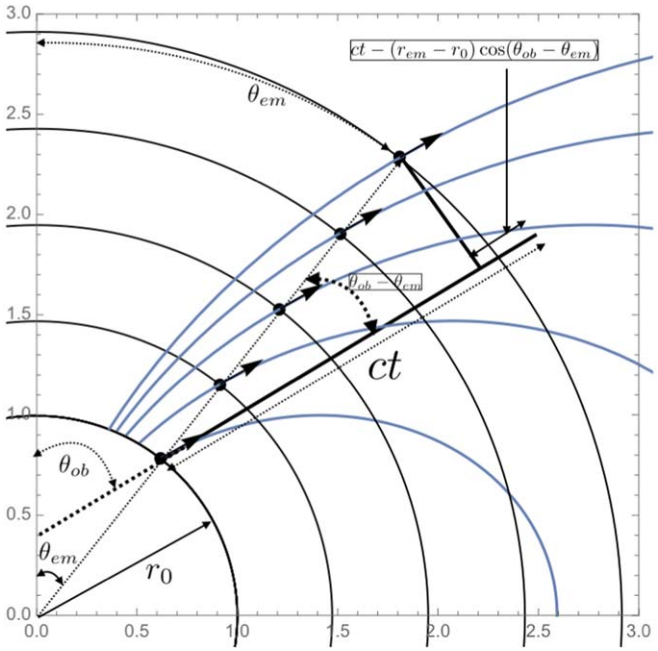

Figure 1. Location of emission points within the magnetosphere. The magnetic axis is vertical. Observer is located at polar angle θ_{ob}, which is time dependent for the rotating case. At time $t = 0$, an emission front is lightened from the surface $r_0 = 1$, propagating along the local magnetic field lines with velocity β. Circles correspond to the radius r_{em} of the emission points at times $t = 0$, 0.5, 1, 2; emission points at each moment are located at radius r_{em} and polar angle θ_{em}; emission is along the local magnetic field. Due to the field lines curvature, the emission front at later times lags behind the one emitted at $t = 0$, even for $\beta = 1$. Observer angle $\theta_{ob} = \pi/4$ in the example pictured. The insert indicates the relation between the observer time and the geometrical parameters.

2. Emission Kinematics with Relativistic and Curvature Effects

2.1. Model Setup

An important concept is the observer time—a time measured from the arrival of the first emitted signal (see, e.g., models of gamma-ray bursts; Piran 2004). In our case, both the relativistic motion and the curved trajectory strongly affect the relation between the coordinate time, t, and the observer time, t_{ob}. To separate effects of rotation from the propagation, we first consider stationary magnetospheres.

Let us assume that at time $t = 0$, an emission front is launched from radius, r_0, propagating with velocity βc along the local magnetic field; Figure 1. Thus, we assume that the whole of the magnetosphere starts to produce emission instantaneously. The trigger could be, e.g., an onset of magnetospheric reconnection event (Lyutikov 2006, 2015). A reconnection event that encompasses the whole region near the surface of the neutron star will be seen at some distance away as a coherent large-scale event. If only a patch of the magnetosphere produces an emission, the light curves will be truncated accordingly. Given that we already have a number of model parameters, we did not explore the finite size of the emission regions in the r–θ–ϕ space.

Let the observer be located at an angle θ_{ob}, measured from the instantaneous direction of the magnetic dipole. Angle θ_{ob} defines a field line with a tangent (the magnetic field) along the LOS at the radius r_0. That field line can be defined by the angle θ_0 of the magnetic foot point. At time t the photons emitted from the surface at $t = 0$ propagated a distance ct. It is assumed

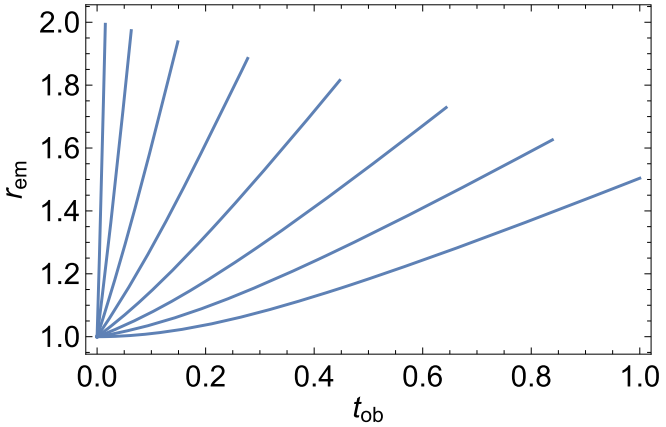

Figure 2. Emission radius as a function of the observer time for different viewing angles, $\theta_{ob} = \pi/8$, $\pi/4$ π; nonrotating magnetosphere; $\beta = 1$, duration of propagation in coordinate time is $\Delta t = 1$. At larger viewing angles, the field lines are more curved: this cancels the relativistic line-of-sight effects, producing longer duration pulses even for $\beta = 1$. (For $\beta = 1$ and $\theta_{ob} = 0$ all emission arrives at $t_{ob} = 0$). For angles $\theta_{ob} > \pi/2$, it is assumed that only "upper" half of the magnetosphere emits.

that at each point emission is produced along the LOS (solid points and arrows in Figure 1). We assume that at given location r_{em} the emission front produces coherent emission at a frequency $\omega(r_{em})$. (We neglect the fact that in a dipolar magnetosphere the strength of the magnetic field at given radius varies by a factor of 2 depending on the magnetic latitude.) As the emission front propagates in the magnetosphere, different magnetic field lines contribute to the observed emission. At time t emission point is located at distance r_{em} and the polar angle θ_{em}. Emission from the point r_{em} arrives at the observer at time t_{ob} that depends on (i) the emission time, (ii) the velocity of the emission front, and (iii) the geometry of field lines.

For a field line parametrized by polar angle θ_0 at r_0, a distance along the field line from θ_0 to $\theta > \theta_0$ is

$$\Delta s = \frac{r_0}{\sin^2\theta_0}\int_{\theta_0}^{\theta}\sqrt{1+3\cos^2\theta}\,\sin\theta d\theta. \tag{3}$$

Emitting particles move according to

$$\Delta s = \beta t, \tag{4}$$

where t is the coordinate time.

The points θ_{em} in the dipolar magnetosphere that have magnetic field along the LOS satisfy

$$\cos 2\theta_{em} = \frac{1}{6}(\sqrt{2}\cos\theta_{ob}\sqrt{\cos(2\theta_{ob})+17} + \cos(2\theta_{ob}) - 1). \tag{5}$$

As Figure 1 demonstrates, the observer time is given by (speed of light is set to unity)

$$t_{ob} = t - (r_{em} - r_0)\cos(\theta_{ob} - \theta_{em}) \tag{6}$$

with $r_{em}(t)$ given by the requirement that particles propagating along the curved field with velocity β emit along the local magnetic field. For nearly straight field lines and highly relativistic velocity, $\beta \approx 1 - 1/(2\Gamma^2)$, the effects of field line curvature dominate for $\theta_{ob} - \theta_{em} \geqslant 1/\Gamma$. (In the calculations

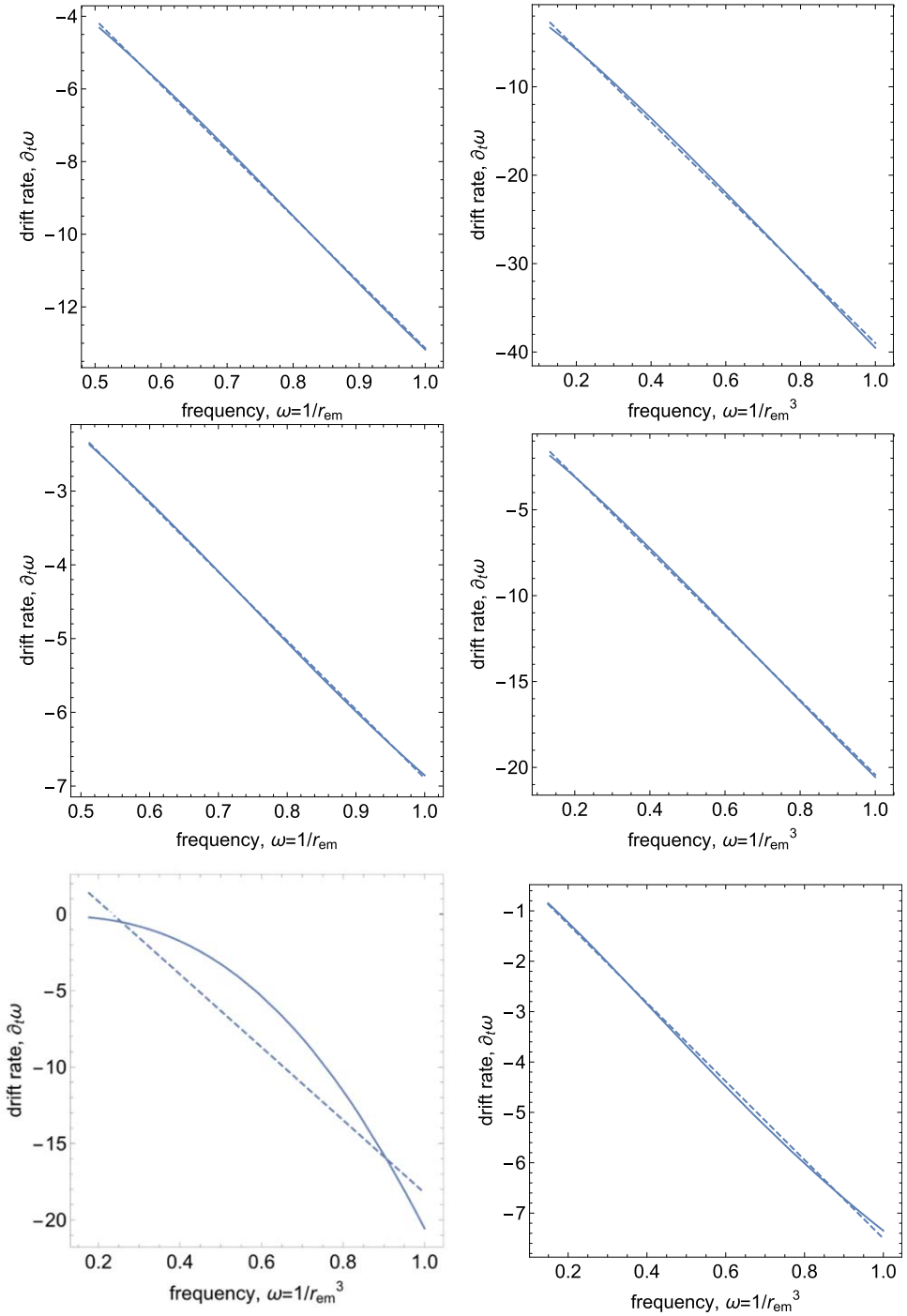

Figure 3. Drift rates in a stationary magnetosphere as function of frequency for two scalings: $\omega \propto r_{em}^{-1}$ (left panels) and $\omega \propto r_{em}^{-3}$ (right panels). Nonrotating magnetospheres. Top row: $\theta_{ob} = \pi/4$; middle row $\theta_{ob} = \pi/3$; and bottom row $\theta_{ob} = \pi/2$. Dashed lines are linear fits $\dot{\omega} \propto \omega$. This simplest case demonstrates that for most observer angles, the frequency drift is linear in time (for smaller θ_{ob}, the drift is more linear, as the fields lines are straighter near the magnetic pole.

below, the time is normalized to unites r_0/c, where r_0 is some initial radius, not necessarily the neutron star radius.)

We then implement the following procedure (see Figure 1):

1. Given is the observer angle θ_{ob} (with respect to the magnetic dipole).
2. Find the polar angle of the footprint $\theta_0^{(0)}$ by solving Equation (5) and setting $\theta_{em} = \theta_0^{(0)}$. (Superscript $^{(0)}$ indicates the moment $t = 0$).
3. After time t the emission front moved along the field lines according to Equations (3) and (4), where $\theta_0(t)$ is a parameter for the field line emitting at time t (at $t = 0$ we have $\theta_0(0) = \theta_0^{(0)}$).
4. For $t \geqslant 0$, using Equations (3)–(5) with $\theta = \theta_{em}$, find the polar angle of the foot point θ_0, Equation (5), where magnetic field is along the LOS at time t.
5. Using Equation (4) find θ_0—the polar angle of the field line that produces emission at time t.

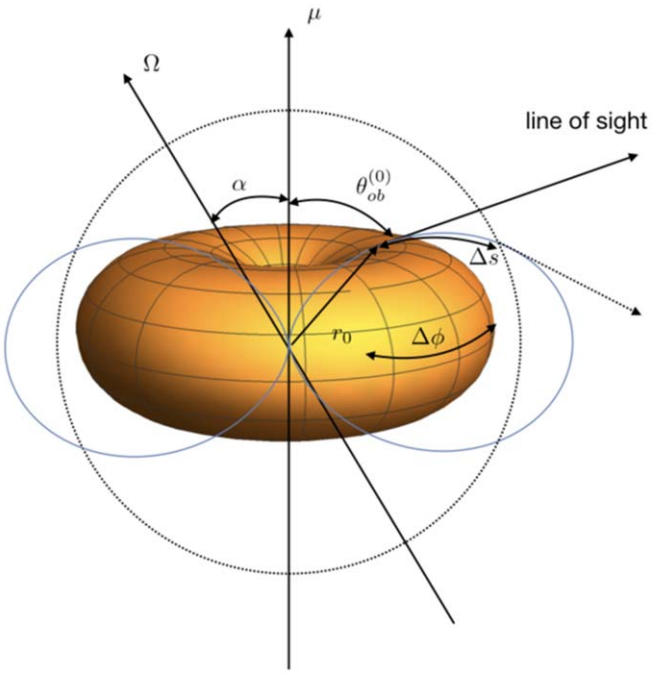

Figure 4. Geometry of the problem at the moment when the LOS is in the μ–Ω plane; the reference frame associated with the neutron star. The magnetic moment is inclined by the angle α with respect to the rotation axis Ω. When the LOS is in the μ–Ω plane, the angle between the LOS and the magnetic moment is $\theta_{\rm ob}^{(0)}$. Emission starts at r_0 (at the moment defined by $\Delta\phi$ and propagates along the local magnetic field, according to $\Delta s = \beta t$. Emission is along the local magnetic field. Later times are denoted by dotted lines. The model is inherently 3D; this picture only illustrate the main geometrical factors.

6. Given time t and the location of the emission point, we can calculate the observer time; see Equation (6).
7. We then find dependence of $r_{\rm em}$ versus $t_{\rm ob}$.
8. Assuming some $\omega(r_{\rm em})$, we find the radius-to-frequency mapping $\omega(t_{\rm ob})$.

Thus, we take into account relativistic transformations and curvature of the field lines in calculating the relations between the observer time versus the coordinate time. We implicitly assume that emitted frequency is the function of the emission radius, $\omega(r_{\rm em})$, but given our uncertainty about the emission properties we do not specify a particulate dependence $\omega(r_{\rm em})$. We plot curves for generic profiles $\omega \propto r_{\rm em}^{-1}$ and $\omega \propto r_{\rm em}^{-3}$; the last scaling is expected if the emission is linearly related to the local magnetic field.

The velocity of the emitting front has a complicated effect on the overall duration of the observed pulse and a range of emitted frequencies. For subrelativistic velocities $\Delta r_{\rm em} \sim \beta \Delta t$ and $t_{\rm ob} \sim \Delta t$. As $\beta \to 1$, the observed duration shortens, $t_{\rm ob} \ll \Delta t$. But for sufficiently high velocity, $\beta \approx 1$ with $\theta_{\rm em} - \theta_{\rm ob} \geqslant 1/\Gamma$, this relativistic LOS contraction become unimportant, as the observed duration is determined by the curvature of field lines.

2.2. Results: Stationary Magnetosphere

In Figure 2, we implement the procedure described above showing $r_{\rm em}(t_{\rm ob})$ for the extreme relativistic limit of $\beta = 1$. This figure demonstrates that the effects of magnetic field line curvature can dominate over the relativistic effects along the LOS.

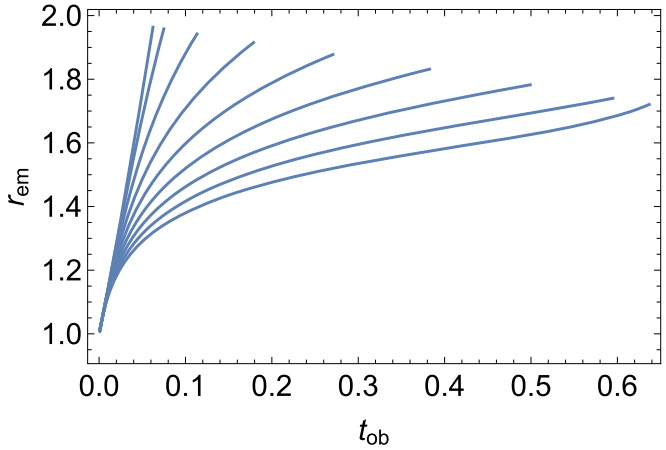

Figure 5. Emission radius as function of the observer time for different $\Omega = 0$, $\pi/8 ... \pi$ (left to right, $\alpha = \pi/4$, $\Delta\phi = 0$, $\theta_{\rm ob} = \pi/2$). This plot demonstrates that faster spin increases the observed duration of a pulse, as the LOS samples larger parameter space.

For assumed scaling $\omega(r_{\rm em})$ $\omega \propto r_{\rm em}^{-1}$ and $\omega \propto r_{\rm em}^{-3}$, the corresponding curves $\omega(t_{\rm ob})$ are given in Figure 3. The model generally reproduces approximate linear drifts rates (see, e.g., Josephy et al. 2019, their Figure 6), regardless of the particular power-law dependence $\omega(r_{\rm em})$. We consider this as a major success of the model.

2.3. Rotating Magnetosphere

We assume next that the star is rotating with spin frequency Ω. The magnetic polar angle of the LOS at time t in the pulsar frame is then

$$\cos\theta_{\rm ob} = \cos\alpha\cos\theta_{\rm ob}^{(0)} + \sin\alpha\sin\theta_{\rm ob}^{(0)}\cos(\Delta\phi + t\Omega), \quad (7)$$

where α is the inclination angle between rotational axis and magnetic moment; $\theta_{\rm ob}^{(0)}$ is the observer angle in the plane comprising vectors of Ω, μ and the LOS; and $\Delta\phi$ is the azimuthal angle of the observer with respect to the Ω–μ plane when the injection starts: this is the phase at $t = 0$. (For example, if emission starts when the LOS is in the Ω–μ plane, at that moment $\theta_{\rm ob} = \alpha - \theta_{\rm ob}^{(0)}$.)

We then implement the procedure outlined in Section 1, with the following modifications; see Figure 4:

1. Given are the $\theta_{\rm ob}^{(0)}$, α, β, Ω, and $\Delta\phi$.
2. For $t \geqslant 0$, implement procedure of Section 1 with time-dependent $\theta_{\rm ob}$ given by Equation (7).

2.3.1. Frequency Drifts in Rotating Magnetosphere

In the rotating magnetospheres, the observed frequency drifts are generally more complicated, as the LOS samples larger part of the magnetosphere. A key limitation in the approach is that we assume that the whole surface $r = 0$ produced as emission front—thus, different parts of the emission front maybe casually disconnected—under certain circumstances this leads to unphysical results (e.g., upward frequency drifts).

In Figure 5, we plot emission radius as function of observer time for different pulsar spins. It is clear that for a given intrinsic burst duration larger Ω produce emission that is seen for a longer observer time. This is due to the fact that the LOS samples larger angular range and correspondingly larger differences in the LOS advances of the emitting region.

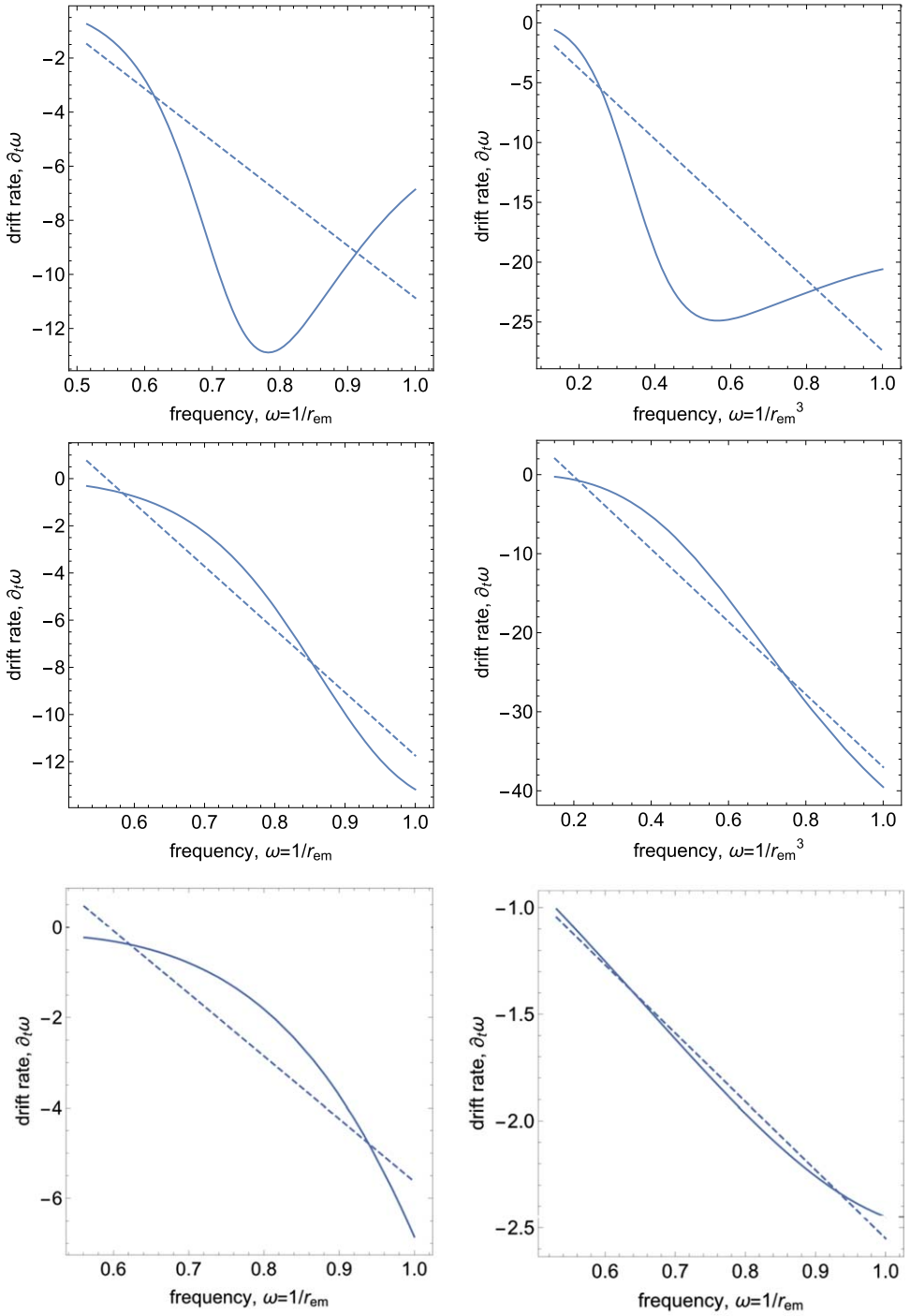

Figure 6. Drift rates as function of frequency in rotating magnetospheres; $\omega \propto r_{em}^{-1}$ (left panels) and $\omega \propto r_{em}^{-3}$ (right panels). Parameters are: $\alpha = \pi/4$, $\theta_{ob}^{(0)} = \pi/2$, $\Omega = \pi 2/$. Top row: $\Delta\phi = -\pi/4$, middle row: $\Delta\phi = 0$, bottom row: $\Delta\phi = -\pi/4$. Dashed lines are linear fits. At intermediate frequencies the drifts rate are highly dependent on the spin frequencies, while at higher frequencies the curves converge and hence less sensitivity to spin. This example shows that the model can produce/predicts a variety of frequency drifts.

In Figures 6 and 7, we show the corresponding frequency drifts for selected parameters. As is clear from the plots, the evolution of the peak frequency can be more complicated in the rotation magnetospheres, as the LOS samples large variations of plasma parameters. (The dimensionless spin $\Omega = \pi/2$ in Figure 6 is relatively high; smaller Ω produce more linear scalings).

Importantly, depending on the trigger phase $\Delta\phi$ the same object will produce different $r_{em}(t_{ob})$ curves; see Figure 8. This explains why in the Repeaters FRB 121102 different burst have different drifts (Hessels et al. 2019). The fact that different parts of the magnetar magnetosphere can become active also explains the lack of periodicity in repeating FRBs.

2.3.2. Prediction: Polarization Swings

Polarization behavior of FBRs is, arguably, the most confusing overall (Masui et al. 2015; Petroff et al. 2015; Caleb et al. 2019; Petroff et al. 2019). We are not interested here in the propagation effects (e.g., sometimes huge and sometimes not rotation measure). There is a clear repeated detection of

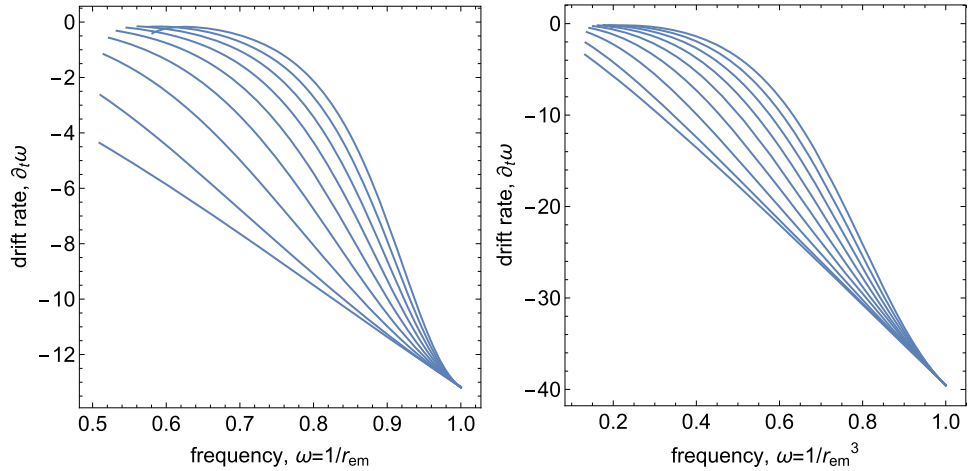

Figure 7. Drift rates as function of frequency in rotating magnetospheres; $\omega \propto r_{em}^{-1}$ (left panel) and $\omega \propto r_{em}^{-3}$ (right panel). Parameters are $\alpha = \pi/4$, $\theta_{ob}^{(0)} = \pi/2$, $\Delta\phi = 0$. Different curves correspond to different spin frequencies $\Omega = 0, \pi/8...\pi$ (bottom to top). Thus, the rotation of a neutron star does affect the frequency drifts. Closer to r_0 (higher frequencies) higher spins result in large frequency drifts.

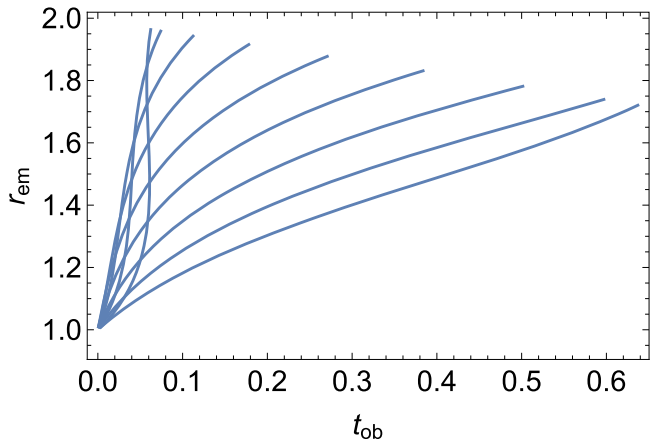

Figure 8. Curves $r_{em}(t_{ob})$ for different launching phases o $\Delta\phi = -\pi/2$–$\pi/2$ in steps of $\pi/8$ ($\alpha = \pi/4$, $\theta_{ob}^{(0)} = \pi/2$, $\Omega = \pi/2$. This demonstrates that different behavior can be seen from the same object depending on the initiation moment of the emission front.

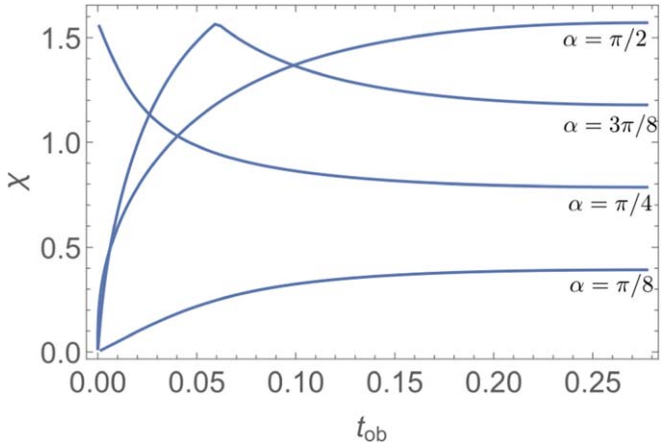

Figure 9. Position angle χ as function ob the observer time t_{ob} for different $\alpha = 0, \ldots\pi/2$ in steps of $\pi/8$; $\Delta\phi = 0$, $\Omega = \pi/2$, $\theta_{ob}^{(0)} = \pi/2$.

linear polarization. Importantly, FRBs have thus far not shown large polarization angle swings (Petroff et al. 2019).

The present model does not address the origin of polarization, as it would depend on the particular coherent emission mechanism. On basic grounds, polarization is likely to be determined by the local magnetic field within the magnetosphere. The model then does predict polarization angle swings. In the rotating vector model (RVM; Radhakrishnan & Cooke 1969) polarization swings reflect a local direction of the magnetic field at the emission point. In our notations, the position angle of polarization χ is given by

$$\tan\chi = \frac{\sin\theta_{ob}^{(0)}\sin(\Omega t + \Delta\phi)}{\cos\alpha\sin\theta_{ob}^{(0)}\cos(\Omega t + \Delta\phi) - \sin\alpha\cos\theta_{ob}^{(0)}}. \quad (8)$$

Generally, we do expect polarization swings through the pulse; see Figure 9. Qualitatively, the fastest rate of change of the position angle occurs when the LOS passes close to the magnetic axis; this requires $\alpha \approx \theta_{ob}^{(0)}$ (so that the denominator comes close to zero). This is the case for rotationally powered pulsars. If emission is generated far from the magnetic axis, the expected PA swings are smaller. Thus, we do predict that PA swings will be observed within the pulses, but with values smaller than the ones seen in radio pulsars.

3. Discussion

In this paper, we further argue that frequency drifts observed in FRBs point to the magnetospheres of neutron stars as the origin (see also Lyutikov 2019b). Our preferred model is a young magnetar-type pulsar producing reconnection events during magnetic relaxation in the magnetospheres (Popov & Postnov 2013). This should be a special type of magnetar, as there are observational constraints against radio bursts associated with the known magnetars (see, e.g., discussion in Lyutikov 2019b)

In an astronomical setting, the repeater FRB 121102 is localized to an active star-forming galaxy, where ones does naturally expects young neutron stars (Tendulkar et al. 2017). In contrast, FRB 180924 is identified with galaxy dominated by an old stellar population with low star formation rate (Bannister et al. 2019). One possibility is the formation of a neutron star from an accretion induced collapse of a white dwarf with a formation of a neutron star; this process is probably responsible for formation of young pulsars in globular clusters (Lyne et al. 1996).

The main points of this work are as follows:

1. The observed drift rate Equation (1) implies sizes of the order of magnetospheres of neutron stars. This is a somewhat

independent constraint on the emission size, in addition to total duration of FRBs (which also is consistent with magnetospheric size).
2. The observed linear scaling of drift rate with frequency, Equation (1), is a natural consequence of radius-to-frequency mapping in magnetospheres of neutron stars. It is valid, generally, for any power-law type $\omega(r_{\rm em})$ dependence. In fast rotating pulsars, the drifts can have more complicated structure; e.g., Figure 7.
3. Nonobservation of drifts in slowly rotating regular magnetars (during radio bursts Maan et al. 2019) is possibly due to the fact that higher spins may lead to higher drift rate (Figure 7), higher amplitude (Figure 2), and longer observer duration (Figure 5).
4. In each given (repeating) FRB, emission can originate at arbitrary rotational phases, resulting in different drift profiles in different pulses from a given repeater; see Figure 8.

The model has a number of predictions:

1. Polarization swings within the bursts, reminiscent of RVM for pulsars, can be observed. The amplitude of the swings in FRBs is expected to be smaller than in radio pulsar, as the emission sights are not limited to the region near the magnetic axis, where PA swings are the largest.
2. For some parameters (LOS, magnetic inclination, and spin) the frequency drifts are not linear in frequency, e.g., Figure 7. Given a limited signal to noise ratio of the typical data, regular, continuous frequency drifts are easier identifiable; more complicated ones are more difficult to find during the de-dispersion procedure. We encourage searchers for more complicated frequency drifts within FRBs.

This work was supported by DoE grant DE-SC0016369, NASA grant 80NSSC17K0757, and NSF grants 10001562 and 10001521. I thank Roger Blandford, Jason Hessels, Victoria Kaspi, and Amir Levinson for discussions and comments on the manuscript.

ORCID iDs

Maxim Lyutikov https://orcid.org/0000-0001-6436-8304

References

Bannister, K. W., Deller, A. T., Phillips, C., et al. 2019, Sci, 365, 565
Caleb, M., van Straten, W., Keane, E. F., et al. 2019, MNRAS, 487, 1191
Cordes, J. M., & Chatterjee, S. 2019, ARA&A, 57, 417
Hessels, J. W. T., Spitler, L. G., Seymour, A. D., et al. 2019, ApJL, 876, L23
Josephy, A., Chawla, P., Fonseca, E., et al. 2019, arXiv:1906.11305
Lorimer, D. R., Bailes, M., McLaughlin, M. A., Narkevic, D. J., & Crawford, F. 2007, Sci, 318, 777
Lyne, A. G., Manchester, R. N., & D'Amico, N. 1996, ApJL, 460, L41
Lyutikov, M. 2002, ApJL, 580, L65
Lyutikov, M. 2006, MNRAS, 367, 1594
Lyutikov, M. 2015, MNRAS, 447, 1407
Lyutikov, M. 2017, ApJL, 838, L13
Lyutikov, M. 2019a, arXiv:1901.03260
Lyutikov, M. 2019b, arXiv:1908.07313
Lyutikov, M., Burzawa, L., & Popov, S. B. 2016, MNRAS, 462, 941
Maan, Y., Joshi, B. C., Surnis, M. P., Bagchi, M., & Manoharan, P. K. 2019, ApJL, 882, L9
Manchester, R. N., & Taylor, J. H. 1977, Pulsars (San Francisco: W. H. Freeman)
Masui, K., Lin, H.-H., Sievers, J., et al. 2015, Natur, 528, 523
Petroff, E., Bailes, M., Barr, E. D., et al. 2015, MNRAS, 447, 246
Petroff, E., Hessels, J. W. T., & Lorimer, D. R. 2019, A&ARv, 27, 4
Phillips, J. A. 1992, ApJ, 385, 282
Piran, T. 2004, RvMP, 76, 1143
Popov, S. B., & Postnov, K. A. 2013, arXiv:1307.4924
Radhakrishnan, V., & Cooke, D. J. 1969, ApJL, 3, L225
Spitler, L. G., Scholz, P., Hessels, J. W. T., et al. 2016, Natur, 531, 202
The CHIME/FRB Collaboration, Amiri, M., Bandura, K., et al. 2019a, Natur, 566, 235
The CHIME/FRB Collaboration, Andersen, B. C., Band ura, K., et al. 2019b, arXiv:1908.03507
Tendulkar, S. P., Bassa, C. G., Cordes, J. M., et al. 2017, ApJL, 834, L7
Wang, W., Zhang, B., Chen, X., & Xu, R. 2019, ApJL, 876, L15